Grain Density-Based Approaches to Predict the Mechanical, Thermal and Hygric Properties of Carbon-Negative Aggregate Concretes

Imen Rahmouni, Geoffrey Promis, Omar Douzane, Frédéric Rosquoet

sustainability

MDPI

Article

Grain Density-Based Approaches to Predict the Mechanical, Thermal and Hygric Properties of Carbon-Negative Aggregate Concretes

Imen Rahmouni [1,2], Geoffrey Promis [3,*], Omar Douzane [3] and Frédéric Rosquoet [3]

[1] Private Higher School of Engineering and Technologies, 1, 2 rue André Ampère B.P. 160-2083—Pôle Technologique—El Ghazala, 1000 Tunis, Tunisia; imen.rahmouni@esprit.tn
[2] Laboratory of Civil Engineering (LGC-ENIT), University of Tunis El-Manar, ENIT-BP 37, 1002 Tunis le Belvédére, Tunisia
[3] Innovative Technologies Laboratory (LTI), University of Picardie Jules Verne, Avenue des Facultés—Le Bailly, CEDEX, 80025 Amiens, France; omar.douzane@u-picardie.fr (O.D.); frederic.rosquoet@u-picardie.fr (F.R.)
* Correspondence: geoffrey.promis@u-picardie.fr

Abstract: The suitability of replacing mineral aggregate with carbon-negative ones mainly depends on the properties of the aggregates produced from waste recycling, reducing CO_2 emissions. This study aimed to investigate the predictive approaches adapted to concrete mixtures where mineral aggregates are replaced by carbonated aggregates (at different substitution rates from 25 to 100% with aggregates of various origins). A large experimental campaign of aggregates and carbonated aggregate concretes highlighted their physical, mechanical, thermal and hygric properties and the influence of density and porosity of aggregates on these properties. Thanks to these results, predictive approaches were formulated to establish the main engineering properties: mechanical compressive strength, elasticity modulus, thermal conductivity, thermal mass capacity and hygric diffusivity. These empirical and analytical models were based on the density of aggregates. Maximum deviations of around 15% were obtained with the experimental data, highlighting the influence of grain density on carbonated aggregate concretes. These models could then be used to optimize the formulation of concrete mixtures with carbonated aggregates, replacing international standards adapted to mineral aggregates.

Keywords: carbonated aggregates; sustainable construction; concrete's multi-physical properties; predictive models

Citation: Rahmouni, I.; Promis, G.; Douzane, O.; Rosquoet, F. Grain Density-Based Approaches to Predict the Mechanical, Thermal and Hygric Properties of Carbon-Negative Aggregate Concretes. *Sustainability* **2021**, *13*, 8194. https://doi.org/10.3390/su13158194

Academic Editor: Gianluca Mazzucco

Received: 28 June 2021
Accepted: 19 July 2021
Published: 22 July 2021

1. Introduction

To meet environmental challenges, one of the current avenues is the valorization of industrial by-products from construction, which is the largest consumer of mineral aggregates. The volume of industrial waste generated and then sent to storage and landfill sites is limited [1]. Indeed, waste from industry can currently be recovered in waste incineration plants in order to use its low entropy to satisfy our energy requirements. Unfortunately, this solution generates waste, bottom ash and fly ash, which are buried in class 3 centers (inert waste). A large volume of waste generates leachates which contain toxic substances (heavy metals and organic compounds . . .) [2]. Landfilling accelerates soil pollution and covers large areas. Thus, the reuse of these industrial by-products would reduce waste production [3–8], while ensuring sufficient sanitary conditions for the construction industry. Another benefit would be the reduction in the consumption of natural resources [9]. The construction sector is the most important consumer of aggregates, the extraction of which is one of the main challenges in the management of non-renewable resources [10]. These non-renewable resources could be, in part, replaced by recycled or bio-based aggregates, to meet the requirements of sustainability [11]. A last benefit would be to improve the energy performance of building envelopes. For that purpose, building

materials based on these aggregates must have hygrothermal characteristics that enhance the energy performance of walls [12] and contribute to the comfort of the occupants [13].

Several approaches are proposed in order to predict the main mechanical performances of concretes regarding the properties of the components of cementitious mixture [14–20]. These approaches were developed using the experimental results of usual and lightweight concrete, which makes them unsuitable for other special concretes. Using carbonated aggregates as a replacement for normal ones improves concrete's thermal properties (conductivity, diffusivity and specific heat capacity) [21]. In order to predict the thermal conductivity for porous materials, there are different theoretical approaches. The most widely used, in the case of building materials, is the model by the auto-coherent homogenization ACH [12,22–25]. The notion of occupant well-being cannot be limited to thermal properties. For these purposes, the identification of the main hygric characteristics of carbonated aggregate concretes is conducted. A simplified theoretical approach of hygric properties (hygric effusivity and diffusivity) is defined [26] to predict the ability of the materials to take up and store moisture.

Thus, in order to encourage designers and engineers to recommend carbonated aggregates, simplified models have to be proposed to predict the main mechanical, thermal and hygric performances of concretes. This study focuses on the influence of carbonated aggregated density on the most significant properties of concretes. To achieve this goal, after a short presentation of carbonated aggregates, a large experimental campaign was presented to identify the properties of aggregates and concretes. These results are then used to formulate some predictive approaches and models based on the current properties of present phases and on the composition of the mixture.

2. Materials and Methods

2.1. Carbonation Aggregates and Environmental Impact

New treatment methods make it possible to transform industrial waste into co-products in order to reduce landfill volumes and reduce the use of non-renewable raw materials. Despite increased recycling, large quantities of waste are not effectively reused, including incineration residues which are often classified as hazardous due to their alkalinity and heavy metal content. One solution is the use of accelerated carbonation technology (ACT) to permanently bind CO_2 into solid carbon by using materials that are naturally reactive, such as waste from thermal processes, due to their high calcium and magnesium content [27]. The accelerated carbonation technology consists of several steps: after being transported and stored at the production facility, the incineration by-products are pre-treated by carbonation and then mixed with cement, sand and water in a carbon dioxide-enriched atmosphere to form a binding paste. The materials are then carbonated in a rotary reactor, forming lightweight aggregates by aggregation around the sand grains. The aggregates produced are then stored and further enriched with CO_2.

Carbonation is obtained by waste exposition to a high concentration of carbon dioxide gas in a controlled environment. The exothermic reaction occurs in the presence of water and gas hydrates of CO_2 to form carbonic acid. CO_2 is first diffused into the solid and then solvated into the pores. In lime-containing materials, such as some wastes, lime hydrates to form calcium hydroxides, thus increasing their reactivity. Then, there is the nucleation of the hydrated calcium silicates CSH and precipitation of the calcium carbonates $CaCO_3$ which act as a binder between the particles. The carbonation in the cementitious matrix presence produces C_3S andC_2S calcium silicates, which interact with carbon dioxide and water due to their hydrophilic character. The reaction will produce $CaCO_3$ which crystallizes into calcite, a stable polymorph under normal conditions, and CSH, a non-crystalline compound [28]. A second carbonation therefore occurs through the decalcification of the CSH to form hydrates and $CaCO_3$:

$$\begin{aligned} C_3S + yH_2O + (3-x)CO_2 &\longrightarrow CxSHy + (3-x)CaCO_3 \\ + zCO_2 &\longrightarrow C(x-z)SHy + zCaCo_3 \end{aligned}$$

These necessary carbonation phases are usually found in many thermal residues and can combine with large amounts of gaseous CO_2 during a short period of time [27]. The entanglement of the CxSHy gel governs the aggregates' strength and participates in inerting the aggregates, thus ensuring the chemical stability of the aggregates. Currently, more than 150 different waste streams were subjected to the accelerated carbonation technology and three different ash supplies have been selected: residues of air-pollution control residues (APCr) ash (C8agg), paper ash (PA) and biomass ash (BAk). Previously dried in an oven, the ashes are then moistened with 10% water and carbonated in a rotating drum under a CO_2-enriched atmosphere and at a constant pressure of 2 bars during 24 h. The process is repeated until a constant mass is obtained, ensuring a saturation in carbonate solution.

A life cycle assessment (LCA) of carbonated aggregates has an excellent environmental performance level due to their ability to store CO_2 during the production process. The environmental impact of carbonated aggregates is assessed according to nine indicators defined by EN 15804. As shown in Table 1, carbonated aggregate production leads to a strong reduction in the eutrophication indicator (−99%) and a 50% decrease in the indicators of soil and water acidification, photochemical ozone formation, resource depletion (elements and fossil fuels) and water pollution. These aggregates also show a negative carbon balance (close to -50 kgCO_2/t).

Table 1. Environmental impact indicators of mineral and carbonated aggregates.

Environmental Indicators	Unit	Aggregates		Δ
		Carbonated	Mineral	
Global warming	(kg CO_2-eq)	259	343	−24%
Ozone depletion	(kg CFC_{11}-eq)	8.82×10^{-6}	8.67×10^{-6}	2%
Acidification of soil and water	(kg SO_2-eq)	0.346	0.643	−46%
Eutrophication	(kg PO_4^{3-}-eq)	0.046	3.800	−99%
Photochemical ozone creation	(kg C_2H_4-eq)	0.024	0.046	−47%
Depletion of abiotic resources—elements	(kg Sb-eq)	1.79×10^{-6}	4.19×10^{-6}	−59%
Depletion of abiotic resources—fossil fuels	(MJ)	603	1400	−57%
Water pollution	(m^3)	5480	9400	−42%
Air pollution	(m^3)	4760	5760	−17%

2.2. Multi-Scale Characterization Methodology

2.2.1. Aggregate Scale

Carbonated aggregates processed from APCr ash (C8agg), paper ash (PA) and biomass ash (BAk) are characterized by standardized methods:

- The identification of granulometry by the sieve method, under dry conditions, according to EN 933-1. The expressions of the differential distributions $q_r(x)$ and cumulative distributions $Q_r(x)$ are given by Equation (1), from the amount of material retained in each sieve's i:

$$Q_{x,i} = \sum_{v=1}^{i} \Delta Q_{x,v} = \sum_{v=1}^{i} q_{x,v} \Delta x_v \quad (1)$$

The granular class of the aggregates is deduced from the interpretation of the granulometric curves, based on the following acceptability criteria:

$$\begin{cases} q_x(D) + q_x(0.63d) \leq & 15\% \\ q_x(1.56D) = & 0 \\ 100 - Q_x(0.63d) \leq & 3\% \end{cases} \quad (2)$$

The granular range can be quantified using the uniformity coefficient Cu and the curve coefficient Cc, whose expressions are:

$$Cu = \frac{Q_{60}}{Q_{10}} \quad (3)$$

$$Cc = \frac{(Q_{30})^2}{Q_{60} \times Q_{10}} \quad (4)$$

where the percentiles, expressed in mm, are deduced from the granulometric curve. The particle size dispersion is translated by the Trask sorting index S_0 and the Folk and Ward skewness index $D_{fw\phi}$, for which the quartiles $Q_{x\phi}$ are the log_2 of the inverse of the percentiles Q_x:

$$S_0 = \sqrt{\frac{Q_{25}}{Q_{75}}} \quad (5)$$

$$D_{fw\phi} = \frac{Q_{84\phi} - Q_{16\phi}}{4} + \frac{Q_{95\phi} - Q_{5\phi}}{6.6} \quad (6)$$

The symmetry of the granulometric curves is approximated by the Krumbein asymmetry index defined as follows:

$$S_{k\phi} = \frac{Q_{25\phi} + Q_{75\phi} - 2 \times Q_{50\phi}}{2} \quad (7)$$

- Measurement of bulk, true and absolute densities by the pycnometric method using toluene in order to limit the risk of mineral dissolution (toluene is a non-polar solvent);
- Calculation of total, interparticle and intraparticle porosities using the following equation system:

$$\varepsilon_{tot} = \frac{\rho_{abs} - \rho_{bulk}}{\rho_{abs}} \quad (8)$$

$$\varepsilon_{inter} = \frac{\rho_{rd} - \rho_{bulk}}{\rho_{rd}} \quad (9)$$

$$\varepsilon_{intra} = \varepsilon_{tot} - \varepsilon_{inter} \quad (10)$$

- Identification of the crush-resistance through a Shimadzu electro-mechanical press with a nominal capacity of 250 kN, equipped with a hollow cylindrical piston (100 mm height and 200 mm^2 cross-section), according to EN 13055-1.

2.2.2. Concrete Scale

Concrete specimens are made with a cementitious binder CEM II/B M(L-S) 32.5 R CE NF by varying the substitution rates of mineral aggregates by carbonated aggregates from 0 to 100% with a 25% step. Special attention is paid to the quantity of water introduced during mixing regarding the high capacity of carbonated aggregates to absorb water, which could influence the quality of the mixture's hydration [29]. An efficient water-to-cement ratio of 0.7 was considered. A 0/5 sand with fineness modulus of 2.5 was used. This sand has a specific density of 2.5. Mineral aggregates are crushed gravel 5/25 with a bulk density of 1150 kg/m^3 and a specific density of 2650 kg/m^3.

Before mixing the various components for 15 min, aggregates were pre-wetted using the amount of water necessary for their absorption capacity. This amount is equivalent to the water absorbed after 30 min of immersion. The aggregates therefore achieve a saturated surface-dry (SSD) condition. Then, natural sand and cement were added. Finally, the mixing water was slowly added and mixed for 4 min. The prepared testing specimens were demolded after 24 h and stored in a chamber with relative humidity ranging from 60 to 80% and a constant temperature of 23 °C [29].

Characterization tests allow the identification of the main mechanical properties: uniaxial compression tests were carried out using a Shimadzu electro-mechanical press with a 250 kN nominal capacity. Each batch test, consisting of three samples of size $\varnothing 11 \times 22$ cm^3 was solicited in simple compression between two parallel plates, hinged at the top. Three potentiometers were used to determine the sample deformation. Tests were performed at 7 days, 28 days, 90 days and one year for each mix of concrete.

A thermal characterization campaign allows the evaluation of the thermal performance of concretes: guarded hot plate (GHP) apparatus is used in order to determine the thermal conductivity. A data logger records the temperature of the cold and hot plates in the central measuring area (25×25 cm^2). A thermopile that measures temperatures in the central and guard zones ensures that the heat flow generated is unidirectional. Samples are pre-dried in a controlled oven at 70 °C, until constant mass is reached. The tests are carried out at average temperatures of 10 °C and a temperature gradient between the hot and cold plates of 10 °C.

A non-steady state method can lead to the determination of several thermal characteristics: for this fluxmetric method, one side of the sample in isothermal condition is subjected to a gradient of temperature. The sample is stabilized at a constant temperature of 15 °C using two thermostatic baths connected to two exchange plates. A temperature gradient of 10 °C is then applied to the upper surface (hot plate). Lateral heat losses are limited by an insulation around the periphery of the sample.

The ability of material to absorb ambient water vapor was identified using sorption isotherms. The adsorption and desorption tests were obtained by using desiccators placed in a thermo-regulated room. Five different levels of relative humidity are generated thanks to specific salts: magnesium chloride, magnesium nitrate, sodium chloride, alumina sulphate and potassium sulphate, which control relative humidities of 33%, 55%, 75%, 81% and 97%, respectively, at 23 °C. The samples used are ($4 \times 4 \times 4$ cm^3) specimens. The wet mass of each sample is regularly measured until it stabilizes, which is a sign of moisture equilibrium.

Finally, a final parameter symbolizing the capacity of a material to regulate the relative humidity can be retained: the moisture buffer value (MBV). The test protocol consists of monitoring the evolution of the wet mass of a sample subjected to moisture solicitation at constant temperature. The cycles of humidity variations follow the protocol defined by the NORDTEST Moisture Buffering Project [30–32], i.e., 8 h at 75% relative humidity and 16 h at 33% relative humidity, with a constant temperature of 23 °C. Samples $10 \times 10 \times 7$ cm^3 of each mix are placed in a temperature and relative humidity controlled chamber (Bia Climatic) and regular weighing (ADAM Nimbus analytical balances) allows the material kinetics to be identified.

3. Experimental Identification of Multi-Physic Properties

3.1. Physico-Mechanical Properties

The sieve size analysis of the three carbonated aggregates is presented in Figure 1). The analysis of the physico-morphological properties of aggregates, summarized in Table 2, proves the possibility of replacing all or part of the mineral aggregates when making concrete. Indeed, carbonated aggregates show a similar size distribution to mineral ones. The grading indices show a proportionate ($D_{f w \phi} \leq 1$) and fairly well-sorted ($S_0 \leq 1.35$) granular distribution, with a high symmetry between the proportions of fine and coarser elements ($S_{k\phi} \simeq 0$). The uniformity and curvature coefficients show that the grain size is well graded and very tight. The granular class, the shape of the curve and sorting indices are very close to those of mineral aggregates. Thus, the morphology of carbonated aggregates does not imply significant differences on concrete behavior. Due to the manufacturing process, all grains have a similar shape (round, governed by the mixing in a rotary reactor) and the grain size analysis tends to demonstrate a similar grain arrangement in concrete regardless of the aggregates.

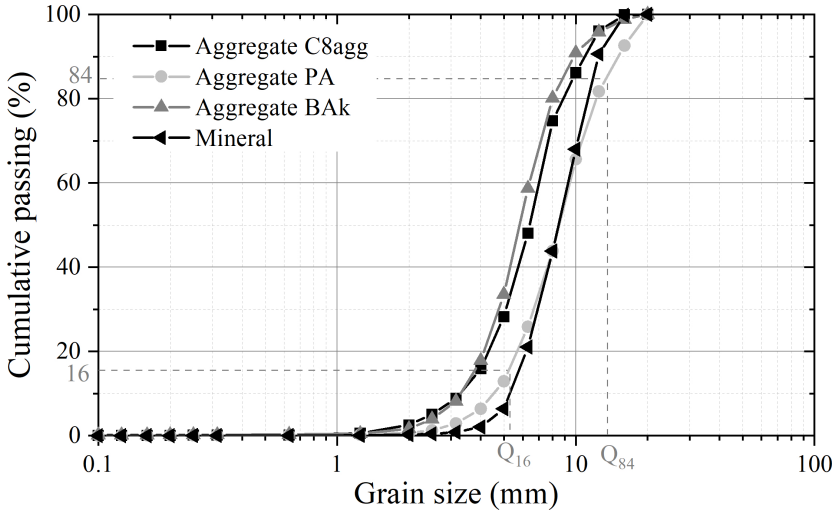

Figure 1. Gradation curves for carbonated aggregates.

Table 2. Aggregates physico-morphological characteristics.

	Aggregate	C8agg	PA	BAk	Mineral
Granular	d	2.5	2.5	2.5	2.5
class	D	16	16	16	16
Shape	Cu	0.53	0.54	0.50	0.65
of curve	Cc	0.95	0.97	0.98	1.09
Sorting	S_0	1.31	1.31	1.36	1.27
indices	$D_{fw\phi}$	0.47	0.62	0.66	0.50
	$S_{k\phi}$	0.03	0.00	0.02	0.02
Density	bulk	1056	779	1186	1362
(kg/m^3)	rd	1816	1541	2040	2500
	absolute	2561	2436	2556	2590
Porosity	total	0.59	0.68	0.55	0.49
(%)	interparticle	0.42	0.50	0.44	0.46
	intraparticle	0.17	0.18	0.11	0.03

The aggregate bulk density is significantly lower than that of a mineral aggregate (close to 1400 kg/m^3) and is governed by a high total porosity. The intraparticle porosity is much higher than that of a mineral aggregate (+200% to +400%). Crush-resistance tests show a linear relationship between the true density of the grain and the crush-resistance coefficient C_a, highlighting the influence of aggregate density on mechanical performance, regardless of the carbonated aggregate:

$$C_a = 7.0 \times \rho_{rd} - 3.6 \quad (11)$$

Figure 2 shows the evolution of the dry density of concretes regarding the amount of carbonated aggregates used in the mix design. Concrete density varies linearly with the substitution rate due to the gradual introduction of air trapped in the internal pores of the carbonated aggregates. The curves representing the density of C8agg and PA aggregate concretes show identical slopes because of the similar intraparticle porosities (0.18 vs. 0.17) when BAk aggregate concrete traps a smaller amount of air ($\varepsilon_{intra} = 0.11$), represented by a lower slope.

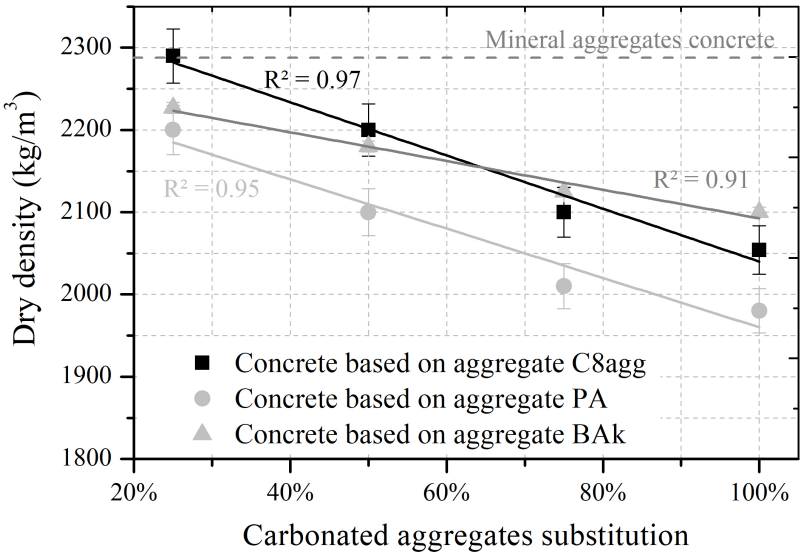

Figure 2. Evolution of the concrete's density regarding the substitution rate with carbonated aggregates.

The average strength of carbonated aggregate concretes is about 16 MPa at 28 days (see Table 3), which seems sufficient for load-bearing structures. As expected, the strength of concrete decreases as the substitution rate of aggregate increases. A significant decrease in the compressive strength of concrete is obtained from a low substitution rate (25%). The introduction of carbonated aggregates generates points of weakness in the granular skeleton, favoring the appearance of the first cracks near these aggregates. The initiation of these cracks then governs an anticipated propagation of cracking leading to the failure of the samples. The theory of the weakest link could explain the asymptotic behavior of the compressive strength of concrete at 1 year at a low substitution rate.

Moreover, C8agg concrete shows the best mechanical strength at one year, followed by BAk concrete and then PA concrete. In the same way as before, the behavior of concrete seems to be dependent of the density of the carbonated aggregates, where C8gg shows a higher density, followed by BAk then PA (Table 2). At 7 days, the differences between concretes are very different. The concrete of PA aggregates shows better mechanical performances than the other two formulations. The crystallization kinematics are impacted by the origin of carbonated aggregates. Aggregates with a high CaO rate (such as that of PA) show the fast formation of Portlandite—and thus the appearance of a crystalline entanglement—which is partly responsible for young age behavior of concrete.

In the same way, the elasticity modulus of concrete is strongly influenced by the introduction of carbonated aggregates in the mix. The carbonated aggregates are porous and have low crushing resistance governing a low modulus of elasticity. Cracks appear within aggregates during compression test representing a good cement matrix-aggregate bonding. Cement paste seems to penetrate into open pores of aggregates, confirming by SEM analysis [29]. The density of aggregates seems to govern the evolution of elasticity modulus which achieves an asymmetrical behavior regarding the substitution rate.

Table 3. Mechanical characterization of the concrete-based carbonated aggregates.

Concrete Based on	Substitution Rate	$f_{c,7}$ (MPa)	$f_{c,28}$ (MPa)	$f_{c,90}$ (MPa)	$f_{c,365}$ (MPa)	$E_{c,28}$ (MPa)
C8agg	100%	7.7 ± 0.62	17.8 ± 1.07	19.9 ± 1.79	23.8 ± 2.14	22.54 ± 2.70
	75%	8.4 ± 0.50	20.1 ± 1.01	21.7 ± 1.74	25.4 ± 3.05	28.65 ± 2.87
	50%	10.9 ± 0.76	20.8 ± 2.29	22.0 ± 2.20	26.1 ± 2.87	30.16 ± 2.11
	25%	19.1 ± 2.29	23.6 ± 1.42	23.4 ± 1.87	26.2 ± 2.36	31.25 ± 3.13
PA	100%	15.2 ± 1.52	16.6 ± 1.33	17.1 ± 1.88	19.8 ± 2.38	23.63 ± 1.89
	75%	15.3 ± 2.60	16.8 ± 1.01	17.2 ± 0.86	18.0 ± 1.08	24.97 ± 3.00
	50%	15.4 ± 1.54	16.8 ± 2.02	17.9 ± 1.97	20.3 ± 3.05	25.32 ± 2.53
	25%	18.5 ± 0.93	21.8 ± 1.18	23.8 ± 1.49	24.3 ± 3.80	28.10 ± 3.37
BAk	100%	10.3 ± 1.75	14.0 ± 1.40	17.6 ± 1.23	20.6 ± 2.88	24.76 ± 1.33
	75%	11.9 ± 0.83	15.6 ± 1.25	18.2 ± 1.64	22.6 ± 3.39	27.14 ± 1.37
	50%	12.3 ± 1.48	16.0 ± 1.28	19.6 ± 1.57	21.0 ± 1.47	28.14 ± 3.38
	25%	12.7 ± 2.29	16.3 ± 0.98	19.8 ± 1.39	21.1 ± 2.11	29.56 ± 3.55
Mineral aggregates	-	26.9 ± 1.34	33.2 ± 1.66	38.5 ± 2.87	42.2 ± 4.22	37.44 ± 3.78

3.2. Thermal Performances

The guarded hot plate test allows for the identification of the experimental thermal conductivity λ_{exp} of bulk aggregates. Due to their intraparticle porosity, the thermal conductivity of carbonated aggregates is lower than that of mineral aggregate (from −40% to −20%). Then, a methodology based on Hashin–Shtrikman limits is used to establish the thermal conductivity of solid phase of aggregates. The performance of a two-phase material is defined as follows [29,33]:

$$\lambda_{agg} = \frac{\lambda_U + \lambda_L}{2} \tag{12}$$

The upper and lower limits of Hashin–Shtrikman, respectively, λ_U and λ_L, can be expressed by the following expressions [24]:

$$\lambda_U = \lambda_s + \frac{\varepsilon}{\frac{1}{\lambda_a - \lambda_s} + \frac{1-\varepsilon}{3\lambda_s}} \tag{13}$$

$$\lambda_L = \lambda_a + \frac{1-\varepsilon}{\frac{1}{\lambda_s - \lambda_a} + \frac{\varepsilon}{3\lambda_a}} \tag{14}$$

where λ_s and λ_a are the thermal conductivity of the solid phase and air, respectively. This approach leads to the thermal conductivity of the aggregate λ_{agg} and of the solid phase of the grain from the total porosity and the interparticle porosity (Table 2). The results presented in Table 4 show the good thermal performance of paper ash-based aggregate (PA) with a bulk thermal conductivity of 0.15 W/(m·K) at 10 °C. The thermal conductivity of a carbonated aggregate remains interesting compared to that of a mineral aggregate (measured close to 0.25 W/(m·K) at 10 °C, with the same experimental protocol) notably because of their high intraparticle porosity.

Table 4. Thermal conductivity of the carbonated aggregates.

Aggregate	λ_{exp} (W/(m·K))	λ_{agg} (W/(m·K))	λ_s (W/(m·K))
C8agg	0.19	0.54	0.90
PA	0.15	0.50	0.92
BAk	0.20	0.59	0.85
Mineral aggregates	0.25	0.84	0.91

The thermal conductivity of the solid part of the grain λ_s is approximately the same for all aggregates, near 0.9 W/(m·K). The intraparticle porosity seems to govern the evolution of the thermal conductivity of the grain λ_{agg} and a linear relation can then be proposed through Equation (15) ($R^2 = 0.92$):

$$\lambda_{agg} = 0.877 - 2.124 \times \varepsilon_{intra} \quad (15)$$

The characterization of the thermal performances of concretes, using the guarded hot plate and fluxmetric methods, is presented in Table 5. The two thermal conductivity measurement protocols lead to a maximum deviation of approximately 10%. Concretes made of carbonated aggregates show an interesting capacity in the storage of energy (through C_p) and a slower propagation of the heat flow by conduction under dynamic conditions (a). The thermal performance seems advantageous, compared to mineral concrete. The identification of thermal conductivity and specific heat capacity lead to the establishment of thermal diffusivity and effusivity.

Table 5. Thermal properties of carbonated aggregate-based concretes.

Concrete Based on	Substitution Rate	λ_d (W/(m·K))	C_p (J/(kg·K))	a (m²/s)	E (J/(m²·K·s$^{1/2}$))
C8agg	100%	0.78 ± 0.08	$1\,640 \pm 262$	0.42×10^{-6}	1134
	75%	0.87 ± 0.09	$1\,263 \pm 208$	0.48×10^{-6}	1178
	50%	1.12 ± 0.11	$1\,200 \pm 203$	0.53×10^{-6}	1239
	25%	1.21 ± 0.12	$1\,025 \pm 185$	0.54×10^{-6}	1310
PA	100%	0.83 ± 0.08	$1\,560 \pm 294$	0.51×10^{-6}	1133
	75%	0.96 ± 0.10	$1\,461 \pm 263$	0.55×10^{-6}	1179
	50%	1.04 ± 0.10	$1\,445 \pm 239$	0.55×10^{-6}	1207
	25%	1.07 ± 0.11	$1\,372 \pm 224$	0.59×10^{-6}	1287
BAk	100%	0.91 ± 0.09	$1\,090 \pm 206$	0.54×10^{-6}	1018
	75%	0.87 ± 0.09	996 ± 196	0.58×10^{-6}	1145
	50%	1.07 ± 0.11	952 ± 188	0.65×10^{-6}	1287
	25%	1.09 ± 0.10	882 ± 182	0.63×10^{-6}	1356
Mineral aggregates	-	1.23 ± 0.07	$1\,815 \pm 283$	0.72×10^{-6}	1449

The use of carbonated aggregates in low proportions (less than or equal to 50%) leads to a small reduction in thermal conductivity compared to standard concrete (greater than 1 W/(m·K)). On the other hand, a higher proportion of carbonated aggregates will have a significant impact with a decrease in the thermal conductivity, lower than 1 W/(m·K). C8 aggregate-based concrete allows to obtain a thermal conductivity lower than 0.8 W/(m·K). These results are explained by the distribution of capillary pores (open and closed) in the concrete. Indeed, mineral aggregate-based concretes present a high thermal conductivity because of the low fraction of air trapped in the pores of the material (matrix and aggregate). For high percentages of carbonated aggregates, the concrete presents a consequent pore network, especially within the aggregates which compose its granular skeleton.

The substitution rate has a significant impact on thermal performance, particularly through the amount of air trapped within the carbonated aggregates. The true density seems to be an interesting property governing the thermal performance of concrete, both for thermal conductivity and thermal mass capacity. On the other hand, the origin of the aggregates does not seem to impact the thermal properties of the concretes, the thermal conductivity of the solid part being appreciably homogeneous among carbonated aggregates (Table 4).

3.3. Hygric Characterization

Figure 3 presents the sorption isotherms at 23 °C of the three carbonated aggregates concretes (100% substitution rate). The large opening of the isotherms shows the capacity

of materials to store and release moisture, thus actively participating in the regulation of the indoor environment relative humidity. The experimental data were fitted by the GAB model. GAB model expresses the evolution of water content as a function of relative humidity, using three experimentally determined parameters, representing the molecular water content w_m, the molar heat of adsorption C and the latent molar heat of vaporization K:

$$u(\varphi) = \frac{w_m C K \varphi}{(1 - K\varphi) \times (1 - K\varphi + CK\varphi)} \quad (16)$$

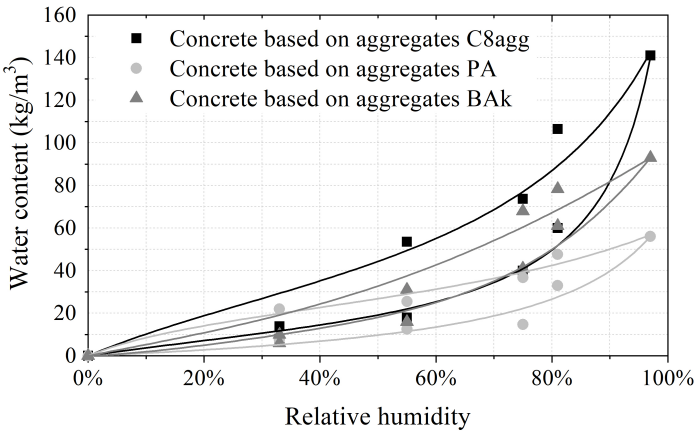

Figure 3. Sorption isotherms of carbonated aggregate-based concretes.

Then, Table 6 summarizes the results of the MBV measurement. In contrast to mineral concrete (which has an MBV close to 1 (g/(m^2·%HR)), corresponding to a moderate capacity to regulate the relative humidity of the environment), carbonated aggregate-based concretes have a good to excellent hygric performance, depending on the substitution rate. As expected with regard to the internal porosity of the grains, the best performances are identified for the highest substitution rates.

Table 6. Moisture buffer value of concretes based on carbonated aggregates.

Concrete Based on	Substitution Rate	MBV_{ads} (g/(m^2·%RH))	MBV_{des} (g/(m^2·%RH))	MBV (g/(m^2·%RH))	Classification
C8agg	100%	2.14	2.62	2.38	Excellent
	75%	1.43	2.38	1.91	Good
	50%	1.80	2.10	1.95	Good
	25%	1.43	2.14	1.79	Good
PA	100%	1.95	2.43	2.19	Excellent
	75%	1.19	1.90	1.55	Good
	50%	1.19	1.67	1.43	Good
	25%	1.11	1.43	1.27	Good
BAk	100%	1.90	2.62	2.26	Excellent
	75%	1.90	2.62	2.26	Excellent
	50%	1.43	2.39	1.90	Good
	25%	1.43	1.90	1.67	Good
Mineral aggregates	-	0.71	1.19	0.95	Moderate

The results show that carbonated aggregates favor water transfer, in liquid or vapor form, because of their microporal structure (quantity and diameter of capillaries). These aggregates then represent a moisture reserve within the concrete itself, governing an ability to regulate the surrounding moisture levels as highlighted by the MBV results.

4. Mechanical, Thermal and Hygric Predictive Approaches

4.1. Empirical Mechanical Model

Conventional approaches of the mechanical properties of concrete tend to over- or underestimate the mechanical characteristics of carbonated aggregates concrete [34]. These approaches lead to the 28-day compressive strength as well as the associated elasticity modulus. Thanks to the experimental campaign, an empirical predictive approach is proposed to assess the main mechanical properties in compression, regarding the density of aggregates. Because of the crystallization times of concretes, depending on the ash origin (Table 3), the approach is focused on the 90-day compressive strength. In a first step, the apparent dry density of the grains ρ^*_{rd} is determined, based on the substitution rate of carbonated aggregates $T_{x,car}$:

$$\rho^*_{rd} = T_{x,car} \times \rho_{rd,car} \cdot \varepsilon_{tot,car} + (1 - T_{x,car}) \times \rho_{rd,min} \cdot \varepsilon_{tot,min} \quad (17)$$

where $\rho_{rd,car}$ can be assessed from the crush-resistance (Equation (11)). Then, the dry density of the formulated concrete ρ_{bd} can be expressed:

$$\rho_{bd} = 2.857 \times \rho^*_{rd} - 1 \quad (18)$$

The mechanical resistance in compression and the associated initial tangential elasticity modulus are deduced:

$$f_{c,90} = 10.96(\rho_{bd} - 0.32) \quad (19)$$

$$E_{c,28} = 17,540\left(\frac{f_{c,90}}{10}\right)^{0.668} \quad (20)$$

Figure 4 shows the comparison between the experimental data and the results from the empirical predictive model. A deviation close to 12% was reached for the compressive strength at 90 days and approximately 10% for the elasticity modulus, in the same order as the uncertainty of mechanical tests (Table 3). This simplified approach, based on the substitution rate and aggregate density, allows an accurate prediction of 90-day strength and tangential modulus of elasticity.

4.2. Prediction of the Thermal Characteristics

As aforementioned, the thermal conductivity of concrete seems to be governed by the true density of aggregates and the substitution rate. In order to confirm that assumption, a thermal model of auto-coherent homogenization (ACH) with tri-composite inclusion is investigated [23]. This model was used to determine the equivalent thermal conductivity of a spherical inclusion comprising three phases. The three phases represent the included air, the solid part of the grain and the binding matrix. In this approach, the material is considered perfectly dry. The thermal conductivity of concrete can be calculated using the input assumptions of the model and the volume concentration coefficients [25]. The concentration coefficients of the ACH model represent the ratio between the different phases, including the impact of grain porosity. The application of the tri-composite ACH model leads to a satisfactory estimation of the thermal conductivity of carbonated aggregate concrete with a maximum deviation between analytical and experimental results of about 20%, as presented in [34]. The concentration coefficients (dependent on the density ratio) mainly govern the model results, regarding the small differences of the thermal conductivity of the solid phase of the carbonated aggregates λ_s. Therefore, a predictive approach is proposed, based on the true homogenized density of the grains ρ^*_{rd} (Equation (17)). Depending on the density of the concrete ρ_{bd} (see Equation (18)), the coefficient χ^* is defined as follows:

$$\chi^* = \frac{\rho_{bd}}{\rho^*_{rd}} \quad (21)$$

This approach allows intraparticle and interparticle porosities to be indirectly taken into account through χ^*. Then, the thermal conductivity of carbonated aggregate-based concrete was expressed by the following expression:

$$\lambda_b = \chi^*(0.18 \times \rho_{bd} + 0.79) \quad (22)$$

Similarly, the thermal mass capacity can be approached as follows:

$$C_p = \chi^* \left(3500 \times \frac{1}{\rho_{bd}} + 3600\right) \quad (23)$$

Modeling results are compared with experimental properties in Figure 5 where a maximum deviation of 10% can be obtained for the thermal conductivity and 11% for the thermal mass capacity, whatever the nature of aggregates and the substitution rate. Thus, the model tends to prove that thermal properties seem to be mainly dependent on grain density, as the nature of ashes to produce carbonated aggregates does not seem to be significant.

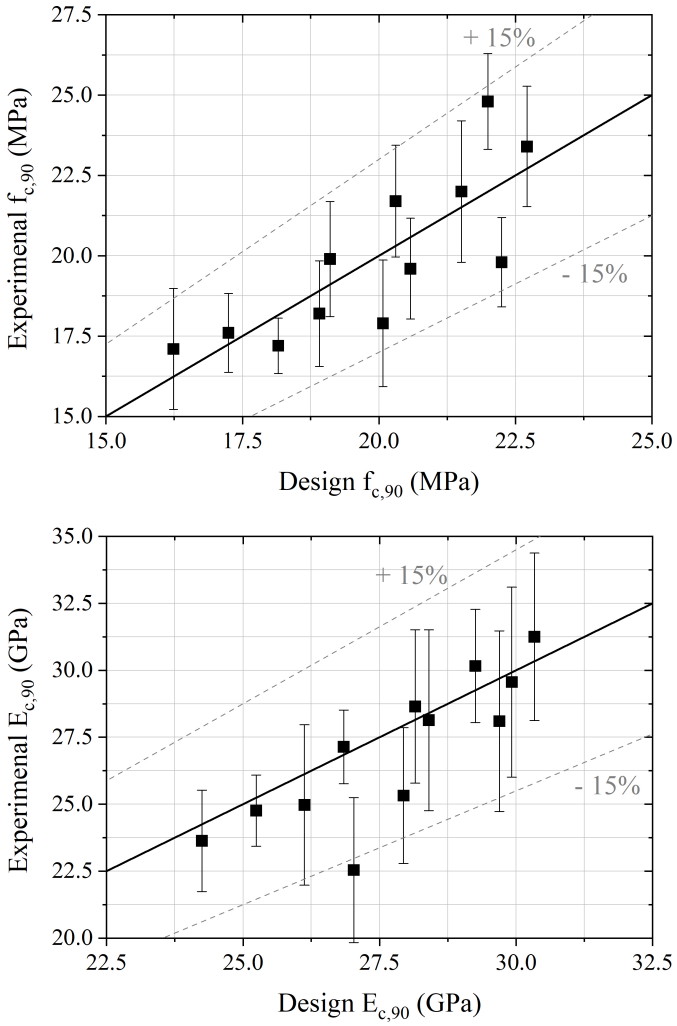

Figure 4. Design mechanical properties compared to experimental ones.

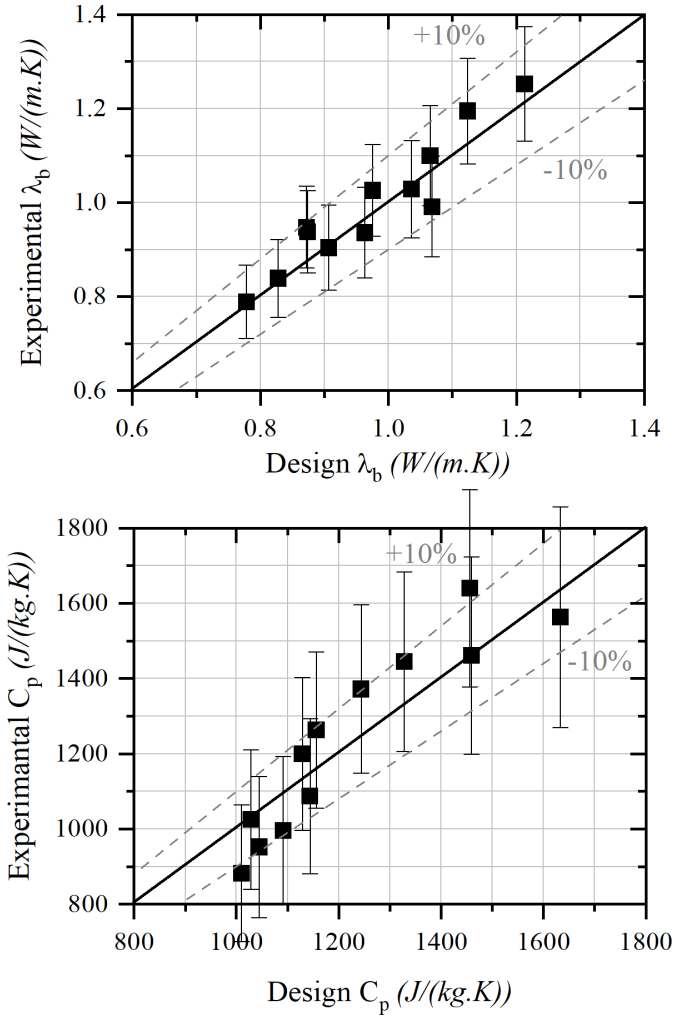

Figure 5. Design thermal properties compared to experimental ones.

4.3. Simplified Theoretical Approach of the Hygric Properties

The NORDTEST Moisture Buffering project protocol defined two theoretical approaches describing the ability of the material to take up and store moisture: hygric effusivity and ideal moisture buffer value. Hygric effusivity is expressed by the following expression [26]:

$$b_m = \sqrt{\frac{\rho_d \times \delta_p \times \xi_\varphi}{P_v^{sat}}} \tag{24}$$

The ideal moisture buffer value corresponds to the MBV for an infinite mass convection coefficient [35]. MBV_{ideal} is thus considered as an intrinsic property of a material and is used to establish the hygric performance of materials [36]:

$$MBV_{ideal} = 0.00568 \times P_v^{sat} \times b_m \sqrt{t_p} \tag{25}$$

The ratio between MBV and MBV_{ideal} is defined as a function of the Biot mass number $B_{i,m}$ [37] which reflects the water vapor diffusion resistance of a material:

$$\frac{MBV}{MBV_{ideal}} = \frac{1}{\sqrt{\left(1 + \frac{1}{B_{i,m}}\right)^2 + \left(\frac{1}{B_{i,m}}\right)^2}} \tag{26}$$

When the Biot mass number tends towards 100, MBV is identical to MBV_{ideal}. For a very low Biot number, MBV tends towards 0. In construction fields, the Biot mass number

is generally between 10 and 100 [35], leading to slight variation of the MBV to MBV_{Ideal} ratio between 0.9 and 1. Assuming an intermediate value of 0.95, a simplified approach leads to the thermal effusivity using the following expression:

$$b_m = \frac{MBV}{0.0054 \times P_v^{sat} \times \sqrt{t_p}} \quad (27)$$

Then, by inverting Equation (24), the coefficient of water vapor permeability can be obtained. This coefficient is necessary to assess the hygric diffusivity D_w, from a semi-infinite homogeneous model [38] where the water capacity is the slope of the sorption isotherm ($\xi_\varphi = \partial u / \partial \varphi$). The water capacity is deduced from Figure 3. Then, the hygric diffusivity is expressed by

$$D_w = \frac{\delta_p \cdot P_v^{sat}}{\rho_d \cdot \xi_\varphi} \quad (28)$$

Table 7 presents the results obtained from this theoretical method, thanks to the hygric characterization campaign. The water capacity corresponds to the current relative humidity range of the building area, between 40 and 80% (where the evolution of water content regarding relative humidity is linear). The vapor diffusion resistance factor μ is the ratio between the vapor permeability of air to the vapor permeability of concrete ($\mu = \delta_a / \delta_p$). This theoretical model leads to a vapor diffusion resistance factor of mineral aggregate concrete near 40 and an hygric diffusion of 5.3×10^{-10} m^2/s, which is in agreement with the literature (see, e.g., the results displayed in [39] which propose a synthesis of the water vapor diffusion coefficient of hardened concretes).

Table 7. Hygric properties of carbonated aggregate-based concretes established from the theoretical approach.

Concrete Based on	Substitution Rate	b_m (kg/(Pa·m²·s$^{1/2}$))	δ_p (kg/(Pa·m·s))	D_w (m²/s)	μ (−)
C8agg	100%	5.33×10^{-7}	4.85×10^{-12}	8.27×10^{-11}	41
	75%	4.28×10^{-7}	2.96×10^{-12}	4.80×10^{-11}	67
	50%	4.37×10^{-7}	2.94×10^{-12}	4.53×10^{-11}	68
	25%	4.01×10^{-7}	2.36×10^{-12}	3.48×10^{-11}	85
PA	100%	4.90×10^{-7}	9.40×10^{-12}	3.67×10^{-10}	21
	75%	3.47×10^{-7}	4.29×10^{-12}	1.53×10^{-10}	47
	50%	3.20×10^{-7}	3.36×10^{-12}	1.10×10^{-10}	60
	25%	2.84×10^{-7}	2.45×10^{-12}	7.40×10^{-11}	82
BAk	100%	5.06×10^{-7}	5.44×10^{-12}	1.16×10^{-10}	37
	75%	5.06×10^{-7}	5.04×10^{-12}	9.91×10^{-11}	40
	50%	4.26×10^{-7}	3.31×10^{-12}	6.07×10^{-11}	60
	25%	3.74×10^{-7}	2.39×10^{-12}	4.10×10^{-11}	84
Mineral aggregates	-	2.13×10^{-7}	4.92×10^{-12}	5.34×10^{-10}	41

The evolution of the vapor diffusion resistance factor regarding the dry density of hardened concrete is plotted in Figure 6, where a linear relation can be highlighted. Thanks to the grain density expressed by Equation (17), the dry density of hardened concrete can be designed (Equation (18)) in order to establish the vapor diffusion resistance factor ($R^2 = 0.94$):

$$\mu = 0.1065 \times \rho_{bd} - 170 \quad (29)$$

Modeling results leads to a maximum deviation of 15%, whatever the origin of carbonated aggregates or substitution rates of mineral aggregates.

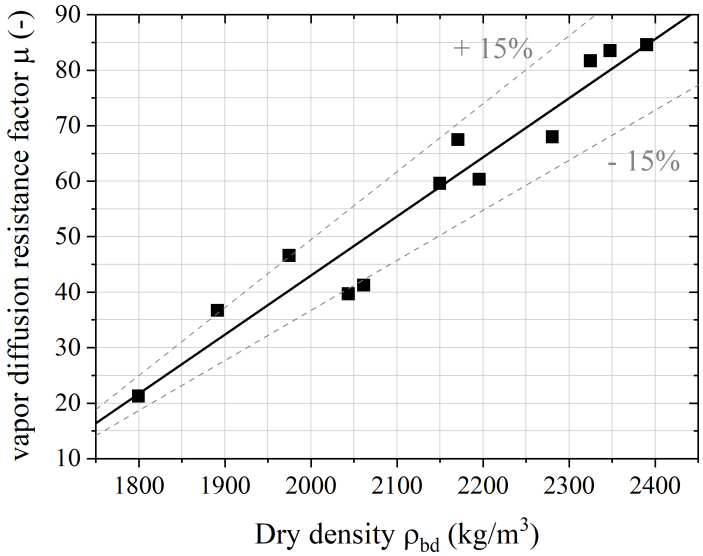

Figure 6. Evolution of the vapor diffusion resistance factor vs. the dry density of concrete based on carbonated aggregates.

5. Conclusions

The use of carbonated aggregates can be focused on limiting the consumption of mineral resources and the quantity of landfill waste. These aggregates are obtained by the carbonation of waste incinerator ashes, and lead to a negative carbon balance. The inclusion of these lightweight aggregates in a cementitious mixture will increase the porosity of the concrete and affects the strength of the structure and the thermal and hygric performances of the building envelope.

Different wastes were used to produce aggregates: APCr ash (C8agg), paper ash (PA) and biomass ash (BAk), chosen from more than 150 waste streams regarding their ability through carbonation. Firstly, concrete samples were produced with an efficient water to cement ratio of 0.7 and using 25%, 50%, 75% and 100% substitution rates of mineral aggregates. Samples were used to identify the main mechanical, thermal and hygric properties of concretes. Experimental results show an improvement of the thermal and hygric performances of concrete, which could lead, in the building fields, to an increase in the thermal insulation (thermal conductivity can be reduced up to 35%) and of the hygroscopic regulation (good to excellent MBV). The mechanical resistance appears sufficient for load-bearing building envelopes (mostly greater than 16 MPa at 28 days).

Moreover, the experimental campaign highlights the influence of the porosity and density of carbonated aggregates on the properties of concrete, for different mix design (substitution rates from 25 to 100%), regardless the water to cement ratio or kind of binder. The origin of carbonated aggregates does not seem to have significant influence on properties of concrete. To confirm that, some predictive laws are proposed to assess the mechanical strength and elasticity modulus of carbonated aggregate concretes, based on the dry density and the porosity of aggregates. This approach leads to a deviation of around 15% compared to experimental results at 90 days. A second model is expressed to predict the thermal conductivity and the specific heat capacity. This model is still based on the density of aggregates. A deviation of around 10% from the experimental data is highlighted. Finally, a simplified theoretical approach was proposed to establish the main hygric properties of concretes, and especially the hygric effusivity and diffusivity in the relative humidity range from 40 to 80%.

Additional experiments could strengthen these models which are developed for carbonated aggregate-based concrete. More tests could be carried out to validate these approaches, with different mixture designs such as the water-to-cement ratio. The valorization of incinerator ashes for building aggregates is still a subject of numerous studies in order to ensure the durability and sustainability of these building materials, as well as the

evolution of thermal and hygric performances over time. In addition, the improvement of tensile performance is critical for making structural concrete. The compatibility with a steel-type reinforcement, in the form of bars or fibers, also appears as an interesting investigative lead.

Author Contributions: Conceptualization, G.P.; methodology, O.D.; validation, I.R.; formal analysis, G.P. and O.D.; investigation, G.P., O.D. and I.R.; writing—original draft preparation, G.P., O.D.; writing—review and editing, I.R. and F.R.; supervision, G.P.; project administration, G.P. All authors have read and agreed to the published version of the manuscript.

Funding: This research received no external funding.

Institutional Review Board Statement: Not applicable.

Informed Consent Statement: Not applicable.

Data Availability Statement: Not applicable.

Acknowledgments: The authors would like to thank partners of the SAPICO$_2$ project which has been selected in the context of the INTERREG European cross-border cooperation program, which is co-financed by the ERDF.

Conflicts of Interest: The authors certify that they have NO affiliations with or involvement in any organization or entity with any financial interest (such as honoraria; educational grants; participation in speakers' bureaus; membership, employment, consultancies, stock ownership, or other equity interest; and expert testimony or patent-licensing arrangements), or non-financial interest (such as personal or professional relationships, affiliations, knowledge or beliefs) in the subject matter or materials discussed in this manuscript. The granting bodies had no role in the design of the study; in the collection, analyses, or interpretation of data; in the writing of the manuscript, or in the decision to publish the results.

Abbreviations

The following abbreviations are used in this manuscript:

ε	porosity
tot	total
inter	interparticle
intra	intraparticle
abs	absolute
rd	true
ρ	density, kg/m^3
a	thermal diffusivity, m^2/s
E	thermal effusivity, J/(m^2·K·s$^{1/2}$)
C_p	specific heat capacity, J/(kg·K)
f_c	compressive strength, MPa
E_c	modulus of elasticity, MPa
car	carbonated
min	mineral
T_x	substitution rate, %
exp	experimental
agg	aggregate
s	solid
D_w	hygric diffusivity, m^2/s
MBV	moisture buffer value, kg/(m^2·%RH)
b_m	hygric effusivity, kg/(m^2·Pa·s$^{1/2}$)
P_v^{sat}	vapor saturation pressure, Pa
δ_p	vapor permeability, kg/(m·s·Pa)

References

1. González-Corrochano, B.; Alonso-Azcárate, J.; Rodas, M. Characterization of lightweight aggregates manufactured from washing aggregate sludge and fly ash. *Resour. Conserv. Recycl.* **2009**, *53*, 571–581. [CrossRef]
2. Behera, M.; Bhattacharyya, S.; Minocha, A.; Deoliya, R.; Maiti, S. Recycled aggregate from C&D waste & its use in concrete—A breakthrough towards sustainability in construction sector: A review. *Constr. Build. Mater.* **2014**, *68*, 501–516.
3. Evangelista, L.; de Brito, J. Mechanical behaviour of concrete made with fine recycled concrete aggregates. *Cem. Concr. Compos.* **2007**, *29*, 397–401. [CrossRef]
4. Poon, C.; Kou, S.; Lam, L. Use of recycled aggregates in molded concrete bricks and blocks. *Constr. Build. Mater.* **2002**, *16*, 281–289. [CrossRef]
5. Rao, A.; Jha, K.N.; Misra, S. Use of aggregates from recycled construction and demolition waste in concrete. *Resour. Conserv. Recycl.* **2007**, *50*, 71–81. [CrossRef]
6. Kayali, O. Fly ash lightweight aggregates in high performance concrete. *Constr. Build. Mater.* **2008**, *22*, 2393–2399. [CrossRef]
7. Radonjanin, V.; Malešev, M.; Marinković, S.; Al Malty, A. Green recycled aggregate concrete. *Constr. Build. Mater.* **2013**, *47*, 1503–1511. [CrossRef]
8. Šavija, B.; Luković, M. Carbonation of cement paste: Understanding, challenges, and opportunities. *Constr. Build. Mater.* **2016**, *117*, 285–301. [CrossRef]
9. Motz, H.; Geiseler, J. Products of steel slags an opportunity to save natural resources. *Waste Manag.* **2001**, *21*, 285–293. [CrossRef]
10. INSEE. *Indicateurs de Développement Durable en Champagne-Ardenne: La Production des Granulats*; Insee dossier n°34; INSEE: Malakoff, France, 2011; pp. 21–22.
11. Chen, T.; Bai, M.; Gao, X. Carbonation curing of cement mortars incorporating carbonated fly ash for performance improvement and CO_2 sequestration. *J. CO2 Util.* **2021**, *51*, 101633. [CrossRef]
12. Cerezo, V. Propriétés Mécanique, Thermique et Acoustique d'un Matériau à Base de Particules Végétales: Approche Expérimentale et Modélisation Théorique. Ph.D. Thesis, Université de Lyon, Lyon, France, 2005.
13. Latif, E.; Lawrence, M.; Shea, A.; Walker, P. Moisture buffer potential of experimental wall assemblies incorporating formulated hemp-lime. *Build. Environ.* **2015**, *93*, 199–209. [CrossRef]
14. BPEL-91. *Régles Techniques de Conception et de Calcul des Ouvrages et Constructions en Béton*; Eyrolles: Paris, France, 1993.
15. Arnould, M.; Virlogeux, M. *Granulats et Bétons Légers*; Presse de l'ENPC: Toulon, France, 1986.
16. ACI Committee 318. *Building Code Requirements for Structural Concrete and Commentary (ACI 318M-11)*; ACI Committee: Farmington Hills, MI, USA, 2011; p. 520. [CrossRef]
17. EN 1992-1-1. EuroCode 2: Design of Concrete Structures: General Rules and Rules for Buildings. 2007. Available online: https://www.phd.eng.br/wp-content/uploads/2015/12/en.1992.1.1.2004.pdf (accessed on 21 July 2021).
18. Zhang, M.; Gjorv, O. Mechanical properties of high-strength lightweight concrete. *ACI Mater. J.* **1991**, *88*, 240–247. [CrossRef]
19. Slate, F.; Nilson, A.; Martinez, S. Mechanical properties of high-strength lightweight concrete. *J. Am. Concr. Inst.* **1986**, *83*, 606–613. [CrossRef]
20. Ke, Y. Caractérisation du Comportement Mécanique des Bétons de Granulats Légers: Expérience et Modélisation. Ph.D. Thesis, Université de Cergy Pontoise, Cergy, France, 2008.
21. Ren, M.; Wen, X.; Gao, X.; Liu, Y. Thermal and mechanical properties of ultra-high performance concrete incorporated with microencapsulated phase change material. *Constr. Build. Mater.* **2021**, *273*, 121714. [CrossRef]
22. Collet, F.; Pretot, S. Thermal conductivity of hemp concretes: Variation with formulation, density and water content. *Constr. Build. Mater.* **2014**, *65*, 612–619. [CrossRef]
23. Rahim, M. Analyse et Caractérisation du Comportement Hygrothermique de Parois Agro-Sourcées à L'échelle 1: Expérimentation et Modélisation. Ph.D. Thesis, Universite de Picardie Jules Verne, Amiens, France, 2015.
24. Hashin, Z.; Shtrikman, S. A variational approach to the theory of the elastic behaviour of multiphase materials. *J. Mech. Phys. Solids* **1963**, *11*, 127–140. [CrossRef]
25. Bederina, M.; Marmoret, L.; Mezreb, K.; Khenfer, M.; Bali, A.; Quéneudec, M. Effect of the addition of wood shavings on thermal conductivity of sand concretes: Experimental study and modelling. *Constr. Build. Mater.* **2007**, *21*, 662–668. [CrossRef]
26. Rode, P. *Moisture Buffering of Building Materials*; Report BYG DTU R-126; Deparment of Civil Engineering Technical University of Denmark: Lyngby, Denmark, 2005.
27. Gunning, P.; Hills, C.; Carey, P. Production of lightweight aggregate from industrial waste and carbon dioxide. *Waste Manag.* **2009**, *29*, 2722–2728. [CrossRef] [PubMed]
28. Fernández Bertos, M.; Simons, S.; Hills, C.; Carey, P. A review of accelerated carbonation technology in the treatment of cement-based materials and sequestration of CO_2. *J. Hazard. Mater.* **2004**, *112*, 193–205. [CrossRef]
29. Rahmouni, I.; Promis, G.; R'mili, A.; Beji, H.; Limam, O. Effect of carbonated aggregates on the mechanical properties and thermal conductivity of eco-concrete. *Constr. Build. Mater.* **2019**, *197*, 241–250. [CrossRef]
30. Rode, C.; Clorius, C. Modeling of moisture transport in wood with hysteresis and temperature dependent sorption characteristics. In *Performance of Exterior Envelopes of Whole Buildings*; International Conference Clearwater: Clearwater, FL, USA, 2004; Volume 80.
31. Rode, C.; Peuhkuri, R.; Time, B.; Svennberg, K.; Ojanen, T. Moisture buffer value of building materials. *J. ASTM Int.* **2007**, *4*, 1–12. [CrossRef]

32. Rode, C.; Holm, A.; Padfield, T. A Review of Humidity Buffering in the Interior Spaces. *J. Therm. Envel. Build. Sci.* **2004**, *27*, 221–226. [CrossRef]
33. Bourdot, A.; Promis, G.; Tran Le, A.; Douzane, O.; Benazzouk, A.; Rosquoët, F.; Langlet, T. Hygrothermal properties of blocks based on eco-aggregates: Experimental and numerical study. *Constr. Build. Mater.* **2016**, *125*, 279–289. [CrossRef]
34. Rahmouni, I. Optimisation de la Formulation de Bétons a Base D'éco-Granulats Obtenus par Carbonatation Accélérée de Déchets D'incinérateur. Ph.D. Thesis, Université de PIcardie Jules Verne, Amiens, France, 2019.
35. Tran Le, A.D. Etude des Transferts Hygrothermiques Dans le Béton de Chanvre et leur Application au Bâtiment: Simulation Numérique et Approche Exp''erimentale. Ph.D. Thesis, Université de Reims Champagne-Ardenne, Reims, France, 2010.
36. Peuhkuri, R.; Rode, C.; Hansen, K.K. Non-isothermal moisture transport through insulation materials. *Build. Environ.* **2008**, *43*, 811–822. [CrossRef]
37. Abadie, M.; Mendonça, K. Moisture performance of building materials: From material characterization to building simulation using the Moisture Buffer Value concept. *Build. Environ.* **2009**, *44*, 388–401. [CrossRef]
38. Arfvidsson, J. Moisture penetration for periodically varing relative humidity at boundary. *Acta Phys. Aedificiorum* **1999**, *2*.
39. Baroghel-Bouny, V. Water vapour sorption experiments on hardened cementitious materials. Part II: Essential tool for assessment of transport properties and for durability prediction. *Cem. Concr. Res.* **2007**, *37*, 438–454. [CrossRef]